fire

MDPI

Article

Study on the Rheological Properties of MC-Based Thermosensitive Gel Foam for Coal Spontaneous Combustion Prevention

Jian Gan [1,2,3,*], Binyi Yang [2], Ning Zhang [4], Shahadad Hossain [5], Dong Ma [6], Yaolin Cao [1,3], Fuchao Tian [3], Hetang Wang [1,5,*] and Xiaolong Zhu [5]

1 State Key Laboratory for Coal Mine Disaster Prevention and Control, China University of Mining and Technology, Xuzhou 221116, China
2 State Key Laboratory for Safe Mining of Deep Coal Resources and Environment Protection, Anhui University of Science and Technology, Huainan 232001, China
3 China Coal Technology and Engineering Group Shenyang Research Institute, Shenyang 113122, China
4 Huayuan Mine, Jining Coal Mining Group Co., Ltd., Jining 272000, China
5 School of Safety Engineering, China University of Mining and Technology, Xuzhou 221116, China
6 State Key Laboratory for Fine Exploration and Intelligent Development of Coal Resources, China University of Mining and Technology, Xuzhou 221008, China
* Correspondence: ganjian@cumt.edu.cn (J.G.); wanghetang@cumt.edu.cn (H.W.)

Abstract

To improve thermoresponsive gel foams for coal spontaneous combustion prevention, the effects of temperature, expansion ratio, and inorganic salts on their rheology, water retention, and film-forming properties were systematically investigated. The results demonstrated that the gel foam exhibited typical yield–pseudoplastic behavior governed by temperature-induced network formation and shear-induced structural disruption. At 60 °C, hydrophobic association promoted a three-dimensional gel network, significantly enhancing apparent viscosity and viscoelasticity and extending the linear viscoelastic region by approximately 11 percentage points compared with 40–55 °C. Under high shear, disruption of the gel network and bubble structure induced pronounced shear thinning, which was well described by the Herschel–Bulkley model. The expansion ratio exhibited a threshold effect: above 4, further increases in viscosity and flow resistance gradually approached saturation owing to the dynamic balance between bubble densification and liquid-film thinning. Inorganic salts regulated foam properties by modifying the gel network and water distribution. Ca^{2+} enhanced network compactness and water retention through a bridging-enhancement/shielding-disruption mechanism coupled with strong hydration, whereas Na^{+} acted mainly through electrostatic shielding. Salt-containing foams exhibited improved water retention but reduced film-forming ability, indicating that foam stability is jointly controlled by interfacial viscoelasticity, network cross-linking, water-state distribution, and gas diffusion. These findings elucidate the rheological regulation of thermoresponsive gel foams under coupled thermal–saline conditions and provide a theoretical basis for designing high-performance materials for coal-fire prevention.

Keywords: coal spontaneous combustion; heat-sensitive; gel; foam; rheology

Check for updates

Academic Editor: Wei Liu

Received: 24 August 2026
Revised: 29 September 2026
Accepted: 8 October 2026
Published: 22 October 2026

Copyright: © 2026 by the authors. Licensee MDPI, Basel, Switzerland. This article is an open access article distributed under the terms and conditions of the Creative Commons Attribution (CC BY) license.

1. Introduction

Coal spontaneous combustion is one of the most serious types of mine fires [1,2]. Its occurrence is characterized by a high degree of concealment, a long reaction period,

and complex multifield coupling, posing a continuous threat to safe coal production and efficient mining of deep resources [1–5]. In particular, due to the scattered distribution of residual coal in the goaf, complex air leakage pathways, and the concealed nature of high-temperature zones, traditional fire-extinguishing agents struggle to be effectively transported to and continuously cover the fire source. Consequently, there is an urgent need for fire prevention and extinguishing materials that combine good flow and permeability, spatial coverage capabilities, and oxygen-blocking performance. Among various fire-suppression materials, foam has attracted considerable attention owing to its low density, high fluidity, and excellent accumulation stability [5,6]. These characteristics enable foam to effectively infiltrate concealed spaces and elevated regions in goafs, forming continuous oxygen-isolating barriers that significantly reduce the risk of coal spontaneous combustion. Consequently, foam-based technologies have become one of the most effective approaches for preventing and suppressing goaf fires [6–9].

Extensive efforts have been devoted to developing foam-based fire-extinguishing materials, leading to the emergence of aqueous two-phase foams, three-phase foams, solidified foams, and colloidal foams with enhanced adaptability to complex coal-fire environments. Early studies by Ray and Smith et al. [10,11] systematically investigated nitrogen-enhanced two-phase foams for coal-fire suppression and demonstrated their superior stability, transportability, and fire-extinguishing performance. However, conventional foam systems suffer from accelerated liquid drainage and bubble collapse under high-temperature conditions, resulting in insufficient long-term stability for sustained fire control [12]. To overcome these limitations, solid particles such as fly ash and cement were incorporated into foam systems to construct three-phase foams with enhanced structural stability and thermal insulation. Qin et al. [13,14] reported that fly ash-based three-phase foams exhibited significantly improved static and dynamic stability compared with conventional two-phase foams, thereby providing superior fire-suppression performance. Similarly, Lu et al. [15] developed a cement-based paste foam capable of maintaining bubble integrity even at approximately 670 K, effectively isolating oxygen and markedly improving the cooling efficiency of coal piles.

More recently, increasing attention has been directed toward the relationship between foam rheology and fire-extinguishing performance. Shi et al. [16] investigated the rheological properties of gel-stabilized foams and demonstrated that the power-law model accurately described their pseudoplastic behavior. Owing to their favorable flowability, gel foams were capable of rapidly penetrating porous media, effectively suppressing concealed fire sources while quickly covering and extinguishing open flames. Xu et al. [17] further showed that inorganic solidified foams behaved as shear-thinning non-Newtonian fluids, with their apparent viscosity and elastic modulus decreasing as the expansion ratio increased, accompanied by an enlarged linear viscoelastic region. Despite these advances, previous studies have primarily focused on the formulation and macroscopic performance of conventional foam materials, whereas the rheological behavior and transport characteristics of thermoresponsive intelligent gel foams in porous media remain poorly understood. In particular, the rheological properties of thermoresponsive foams determine their structural stability under shear and seepage conditions, thereby affecting their migration ability, coverage efficiency, and plugging performance within porous coal seams. These properties are essential for suppressing coal spontaneous combustion and enhancing the efficiency of coal-fire prevention and control [18–20].

Motivated by these considerations, this study systematically investigates the effects of temperature, expansion ratio, and inorganic salt ions on the rheological behavior, viscoelasticity, water-retention capacity, and film-forming properties of thermoresponsive gel foams. A constitutive rheological model is further developed to characterize their

flow behavior, and the mechanisms governing the rheological response under thermal, foaming, and saline conditions are elucidated. The findings provide a mechanistic basis for understanding the structure–property relationships of thermoresponsive gel foams and offer theoretical guidance for the design and optimization of high-performance foam materials for coal-fire prevention and control.

2. Materials and Methods

2.1. Materials and Foam Fluids Preparation

Thermosensitive gel foam is primarily composed of a cross-linking agent ($Na_2B_4O_7$), a foam stabilizer (MC), foaming agents (APG and ALES), and a small amount of additives. Specifically, $Na_2B_4O_7$ and MC were sourced from Tianjin Hengxing Chemical Reagent Manufacturing Co., Ltd. (Tianjin, China), while APG and ALES were obtained from Shandong Yousuo Chemical Technology Co., Ltd. (Linyi, China). Detailed parameters are provided in reference [21]. Gel foams with different foaming ratios were prepared using a stirrer (see Figure 1). Coal mine water is mostly treated circulating mine water, which contains a large amount of Na^+, Ca^{2+}, Mg^{2+}, Cl^- and other ions. Therefore, solutions with different salt ion concentration gradients were prepared using $CaCl_2$ and NaCl to evaluate the effect of salt ions on the rheology of gel foam [22–24]. Considering the water-quality composition and hardness of the mine water, we selected Na^+ and Ca^{2+} concentrations of 100 mg/L, 200 mg/L, 400 mg/L, 800 mg/L, and 1000 mg/L for testing.

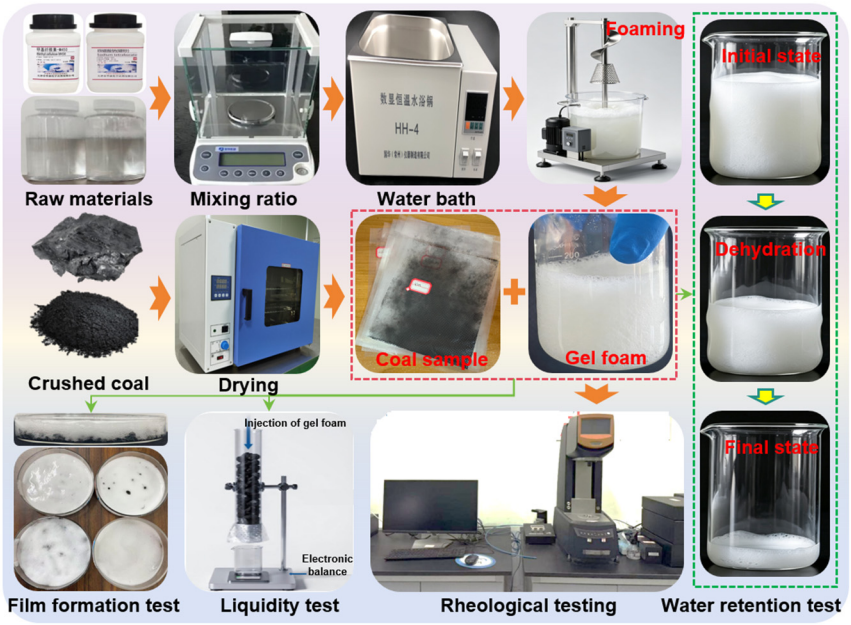

Figure 1. Experimental procedure.

2.2. Foam Rheology Experiment

The rheological properties of the gel foam were tested using a DHR thermal conductivity viscoelastic rheometer. Flow mode and oscillation mode were selected to test the viscosity changes with shear rate, as well as the storage modulus and loss modulus of the material [16]. Considering the phase transition temperature of MC, we selected 40 °C, 45 °C, 50 °C, 55 °C, and 60 °C as experimental temperature points to conduct research. The experimental conditions, such as normal force, angular frequency, and angular velocity, were set to 0.005~50 N, 7~628 rad/s, and 9~314 rad/s, respectively, and the shear rate was set to 0.1 s^{-1}~100 s^{-1}.

2.3. Foam Percolation Experiment

A circular tube percolation experimental platform was constructed, consisting of a transparent acrylic circular tube (inner diameter 40 mm, height 500 mm), an electronic balance, and beakers. The interior of the circular tube was filled with 120 g of lump coal (particle size: 15–20 mm), and a seepage channel was provided at the bottom of the tube. Gel foam (250 g) containing $CaCl_2$ (1 g/L) and NaCl (1 g/L) was poured into the round tubes, and gel foam without salt ions was used for comparison. Timing began when gel seeped out and stopped after 100 min, with the weight of the gel in the beaker recorded in real time.

2.4. Foam Water Retention and Film Formation Experiment

Two 100 g samples of gel foam—one containing 0.1% $CaCl_2$ and the other 0.1% NaCl—were placed under identical environmental conditions (temperature 25 °C, humidity 40%), with gel foam containing no salt ions serving as the control. They were weighed every 24 h, and the mass change was recorded. Smaller mass changes indicated stronger water retention. For the film formation experiment, a coal sample was first evenly spread in a glass petri dish, and then the three types of gel foam were evenly covered on the surface of the coal sample. Changes were recorded every 6 h.

3. Results and Discussions

3.1. Steady-State Rheological Analysis of Thermosensitive Gel Foam

Temperature is a critical factor influencing the rheological behavior of thermosensitive gel foam. Underground coal mines—particularly in goaf areas and in the vicinity of fire sources—exhibit significant temperature gradients; as thermosensitive gel foam is transported and undergoes seepage, it experiences transitions from ambient to high temperatures, resulting in marked changes in viscosity and fluidity. Rheological testing across various temperatures allows for the simulation of underground thermal conditions and the elucidation of the foam's structural response and transport characteristics, thereby providing a basis for evaluating its injectability, stability, and suitability for high-temperature fire control.

Based on steady-state flow experiments, a comparative analysis of the rheological behavior of gel foam at different temperatures was conducted, with results presented in Figure 2a. All five fluids exhibited similar rheological characteristics, with shear stress increasing significantly as the shear rate rose. Figure 2a reveals that the gel foam displays typical shear-thinning behavior characteristic of non-Newtonian fluids; the shear rate versus shear stress curves are not straight lines passing through the origin. The stress curves for the 40 °C to 60 °C range show similar upward trends, with shear stress increasing alongside the shear rate. Between 40 °C and 55 °C, the shear stress of the foam fluid showed a distinct upward trend with rising temperature, though the variations in the shear rate–shear stress curves were minimal within this range. The initial shear stress values ranged from 6 Pa to 9 Pa between 40 °C and 55 °C, whereas the initial stress at 60 °C (33.12 Pa) was significantly higher.

As shown in Figure 2b, at low shear rates (0.1 s^{-1}), the relatively small viscosity variation between 40 and 55 °C suggests that extensive thermogelation had not yet occurred. At relatively low temperatures, hydrogen bonding between the residual hydroxyl groups of MC and surrounding water molecules favors chain hydration and maintains a comparatively weakly associated state [25]. As temperature increases, progressive dehydration of the substituted MC chains weakens polymer–water interactions and promotes the association of hydrophobic methoxy-rich regions [26]. At 60 °C, enhanced hydrophobic association facilitates physical cross-linking and the development of a three-dimensional

network, resulting in the pronounced increase in apparent viscosity. This interpretation is consistent with previous studies showing strong thermally induced association and rheological transitions of aqueous MC systems around the gelation regime [27]. With increasing shear rate, however, the apparent viscosity decreased markedly, indicating pronounced shear-thinning behavior. The imposed shear promotes chain alignment and disrupts weak reversible associations within the MC network, while simultaneously inducing bubble deformation and structural rearrangement within the foam, thereby reducing resistance to flow [28]. Consequently, at 100 s^{-1}, the apparent viscosities at different temperatures converged toward relatively low values, indicating that shear-induced structural disruption progressively outweighed the temperature-induced strengthening of the gel network.

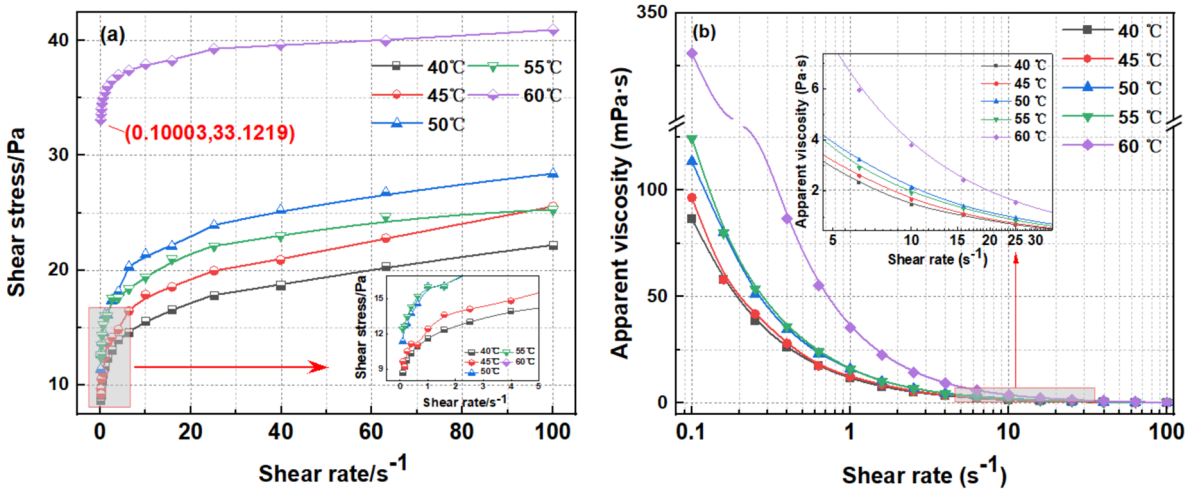

Figure 2. Rheological curves of gel foam fluid at different temperatures. (**a**) shear stress, (**b**) apparent viscosity.

3.2. The Rheological Constitutive Equation of Thermosensitive Gel-Foam Fluid

Fluids can be classified as Newtonian or non-Newtonian based on whether they obey Newton's law of internal friction. A Newtonian fluid is one whose viscosity remains constant at a given temperature across a wide range of shear rates. In contrast, non-Newtonian fluids exhibit a nonlinear relationship between shear stress and shear rate, with viscosity varying in response to changes in either shear stress or shear rate. Non-Newtonian fluids are further categorized into time-dependent and time-independent types, depending on whether the viscosity coefficient depends on the duration of shearing. Time-independent non-Newtonian fluids are classified into three categories: plastic, pseudoplastic, and dilatant fluids.

Figure 3a illustrates the relationship between shear stress and shear rate for these various fluids. Rheological studies indicate that gel foam exhibits shear-thinning behavior and is a typical time-independent non-Newtonian fluid. Therefore, the Bingham, Power-law, and Herschel–Bulkley models—commonly used in the field—are employed to investigate the rheological behavior of the thermosensitive gel foam. First, the rheological curve of the gel foam fluid is fitted using the Bingham model [29].

$$\tau = \tau_B + \mu_B \gamma \quad (1)$$

In the equations, τ, γ, τ_B, and μ_B represent shear stress, shear rate, yield stress, and the stress coefficient, respectively. As shown in Figure 3 and Table 1, the rheological curve of the gel foam fluid increases monotonically and is concave downward, whereas the fit for the Bingham fluid model yields a straight line with R^2 values below 0.9 and

significant fitting errors; clearly, this model is unsuitable. Analysis of the shear rate–shear stress curves for the gel foam fluid at various temperatures indicates that its rheological behavior closely matches that of a pseudoplastic fluid. To quantitatively describe the effect of temperature on foam flow characteristics and to improve the accuracy of rheological parameter characterization, the experimental data were fitted using the Power-law model (Equation (2)) [30] and the Herschel–Bulkley model (Equation (3)) [31]; the latter accounts for yield stress effects.

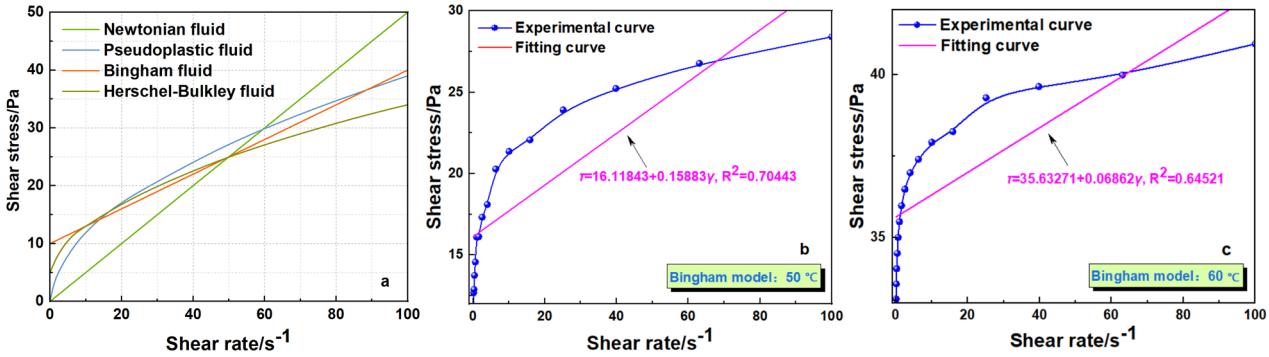

Figure 3. (**a**) Variation of shear stress with shear rate for different fluids; fitting results of the Bingham model for gel-stabilized foam fluids: (**b**) 50 °C; (**c**) 60 °C.

Table 1. Bingham model fitting parameters and rheological constitutive equation.

Temp. /°C	Fitting Results			
	Rheological Constitutive Equation	τ_B	μ_B	R^2
40	$\tau = 15.09476 + 0.07954\gamma$	15.09476	0.07954	0.85082
45	$\tau = 12.96010 + 0.15278\gamma$	12.96010	0.15278	0.75648
50	$\tau = 16.11843 + 0.15883\gamma$	16.11843	0.15883	0.70443
55	$\tau = 16.00095 + 0.12296\gamma$	16.00095	0.12296	0.70275
60	$\tau = 35.63271 + 0.06862\gamma$	35.63271	0.06862	0.64521

The shear rate–shear stress equations for the Power-law and Herschel–Bulkley models are as follows:

$$\tau = K\gamma^n \quad (2)$$

$$\tau = \tau_B + K\gamma^n \quad (3)$$

In the equation, τ, γ, K, n, and τ_B represent shear stress, shear rate, consistency coefficient, non-Newtonian flow behavior index, and yield stress, respectively.

As shown in Figure 4, the fitted curves align well with the experimental curves, and the fitting parameters are listed in Tables 2 and 3. The Power-law model fitting results indicate that the flow consistency index (K) of the solution increases gradually with temperature; while the K values show little variation within the 40–55 °C range, the value at 60 °C is two to three times higher than under other conditions. This suggests a significant phase transition in the foam fluid at 60 °C, consistent with the conclusions drawn in Section 3.1. Furthermore, an analysis of the non-Newtonian flow behavior index (n) reveals that the foam fluid exhibits more pronounced non-Newtonian rheological characteristics at higher temperatures. Additionally, as illustrated in Figure 4 and Table 3, the R^2 values obtained using the Herschel–Bulkley model at various temperatures are generally superior to those of the Power-law model, indicating that the Herschel–Bulkley model more accurately captures the yield characteristics and shear-thinning effects of the thermosensitive gel foam system. This result aligns with findings in non-Newtonian fluid rheology: the Herschel–Bulkley

model combines the yield-stress term (τB) of the Bingham model with the nonlinear flow behavior described by the Power-law index (n < 1) [32]. Specifically, τB represents the critical stress required to overcome the interconnected gel–bubble network and initiate macroscopic flow, while (n < 1) quantitatively reflects the post-yield shear-thinning behavior [32–34]. Thus, the model simultaneously captures the yield resistance of the structured foam and its nonlinear flow response after yielding, overcoming the limitations of the Bingham model in describing nonlinear post-yield behavior and of the Power-law model in accounting for yield stress [32]. This physical interpretation is consistent with the characteristic rheological behavior of structured foams, which generally exhibit a finite yield stress followed by shear-thinning flow [33,34]. Therefore, the thermosensitive gel foam can be appropriately classified as a yield–pseudoplastic fluid, and the Herschel–Bulkley model provides a physically meaningful description of its rheological behavior. Accordingly, the temperature-dependent constitutive equations were established, as summarized in Table 3.

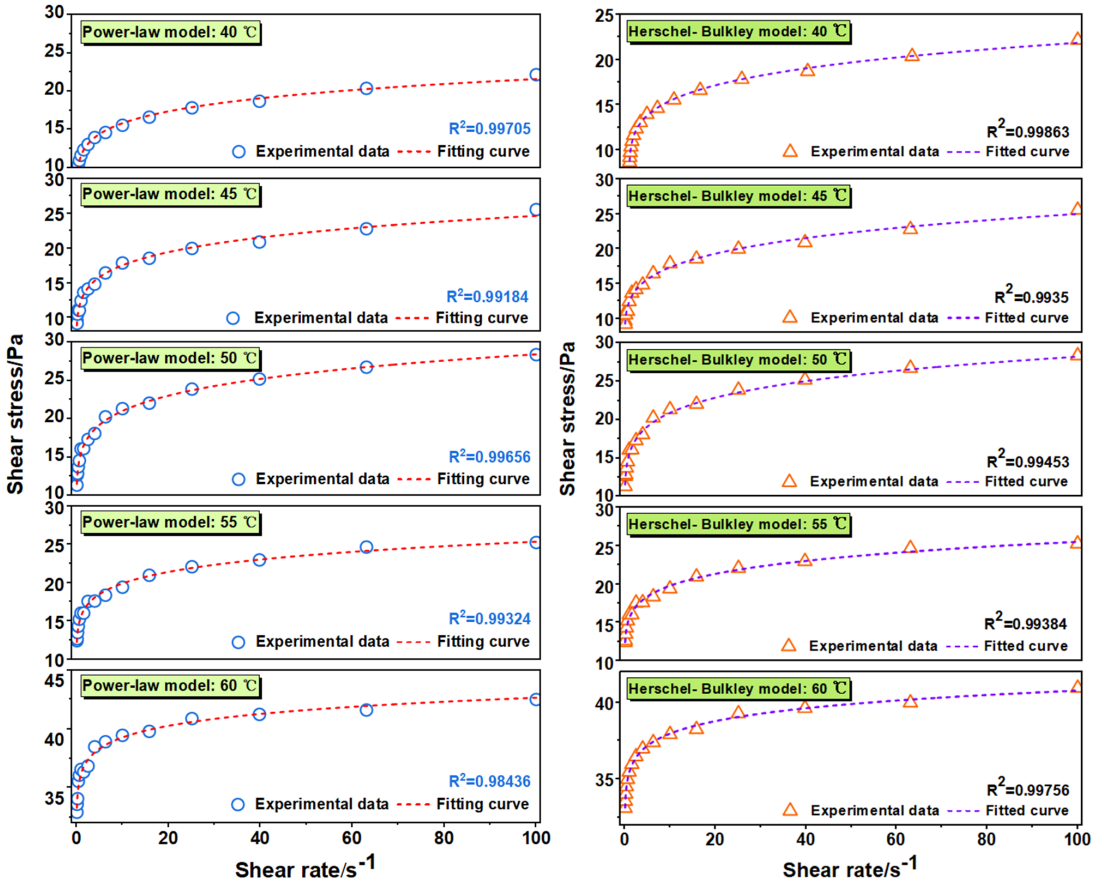

Figure 4. Fitting results of the Power-law and Herschel–Bulkley models for thermosensitive gel foam fluids at different temperatures.

Table 2. Fitting parameters and rheological constitutive equation of Power-law model.

Temp./°C	Fitting Results			
	Rheological Constitutive Equation	*K*	*n*	R^2
40	Y = 11.5962γ0.13501	11.5962	0.13501	0.99705
45	Y = 12.48468γ0.14772	12.48468	0.14772	0.99184
50	Y = 15.56803γ0.13086	15.56803	0.13086	0.99656
55	Y = 15.62425γ0.10523	15.62425	0.10523	0.99324
60	Y = 36.17469γ0.03576	36.17469	0.03576	0.98436

Table 3. Fitting parameters and rheological constitutive equation of the Herschel–Bulkley model.

Temp./°C	Fitting Results				
	Rheological Constitutive Equation	τ_B	K	n	R^2
40	$Y = 3.45517 + 8.07771\gamma 0.17907$	3.45517	8.07771	0.17907	0.99863
45	$Y = 3.60102 + 8.8151\gamma 0.19254$	3.60102	8.8151	0.19254	0.9935
50	$Y = 0.48042 + 15.07108\gamma 0.1327$	0.48042	15.07108	0.1327	0.99453
55	$Y = 3.61886 + 11.95675\gamma 0.13164$	3.61886	11.95675	0.13164	0.99384
60	$Y = 11.84028 + 23.61122\gamma 0.04421$	11.84028	23.61122	0.04421	0.99765

3.3. Viscoelastic Properties of Thermosensitive Gel Foams Under Amplitude Sweep Conditions

Amplitude sweeps involve the application of progressively increasing strain (amplitude) at a constant frequency to determine how the storage modulus (G′), loss modulus (G″), and phase angle (δ) of the gel foam vary with strain; this process evaluates the foam's linear and nonlinear viscoelastic behavior under oscillatory strain and characterizes its resistance to deformation and foam stability. G′ refers to the amount of energy stored due to elastic deformation (reversible) when the material deforms, reflecting the elasticity of the material, and G″ represents the amount of energy lost due to viscous deformation (irreversible) when the material deforms, reflecting the viscosity of the material [35].

Figure 5 demonstrates that when the oscillatory strain is small, the G′, G″, and δ values of the sample remain essentially unchanged. At this time, the sample is in the linear viscoelastic range; when the applied force or deformation exceeds the critical point, a certain degree of damage occurs inside the sample and the modulus decreases. Generally, the larger the elastic modulus, the more stable the sample, and the foam system can withstand greater deformation without being destroyed. In the low-strain range, δ is less than 45°, and G′ > G″. The sample's structural properties are close to those of a viscoelastic suspension or viscoelastic solid, indicating a solid-like state with a certain degree of hardness and stability. As the strain increases, the δ value gradually increases, and finally exceeds 45°. At this stage, G′ < G″; the internal structure of the sample system is weak, and the properties approach those of a viscoelastic liquid, showing a flow-like state [36]. When δ is equal to 45°, the corresponding point is the intersection of G′ and G″. Under this oscillatory strain condition, the internal structure of the gel foam is largely destroyed. It is worth noting that G′ begins to decrease when the oscillatory strain of the gel foam reaches about 5.6% at 40–55 °C; it needs to reach about 16.621% at 60 °C before G′ starts to decrease. The results indicate that, compared to 40–55 °C, the linear viscoelastic range of the gel foam expanded by approximately 11 percentage points at 60 °C. This is because the gel phase transformation of the gel foam at 60 °C causes relatively low energy dissipation during the deformation process and exhibits relatively stable viscoelastic behavior.

The crossover of G′ and G″ marks the transition from an elasticity-dominated viscoelastic response to a viscosity-dominated one. The gel foam reached the critical point at 46.98% oscillatory strain at 40 °C, with a modulus value of 28.55 Pa, while the critical strain of the foam increased to 48.3% at 60 °C, with a modulus value of 42.02 Pa. This shows that, at 40 °C, the foam has poor elastic energy storage capacity and slightly weaker vibration resistance, while at 60 °C it can maintain excellent elastic energy storage characteristics under large oscillating strains, exhibiting stronger vibration resistance. It is worth noting that although the oscillatory strains corresponding to the intersection points of G′ and G″ of the foam at 50 °C and 55 °C are both smaller than those at 40 °C and 60 °C, their modulus values are significantly higher than 40 °C and 60 °C. This indicates that, at 50 °C and 55 °C, the foam has a weak ability to resist oscillatory strain, and viscoelastic transformation can occur under higher modulus conditions. We speculate that this is because the temperature

range of 50 to 55 °C corresponds to the structural reorganization stage before the foam phase transition. At this stage, the thermal movement of molecules promotes frequent contact of the MC polymer chains, forming more transient association points. Local cross-linking effects, such as hydrogen bonds and hydrophobic associations between molecular chains, are enhanced, which increases the instantaneous stiffness of the foam system and increases the G′ and G″ values. However, the cross-linked network formed at this stage is not completely continuous and stable, the structural uniformity is poor, and local stress concentration is clear. When subjected to external oscillations, the cross-linked network is prone to damage under small strains, so the critical oscillation strain corresponding to the intersection point of G′ and G″ is small, but the corresponding modulus increases.

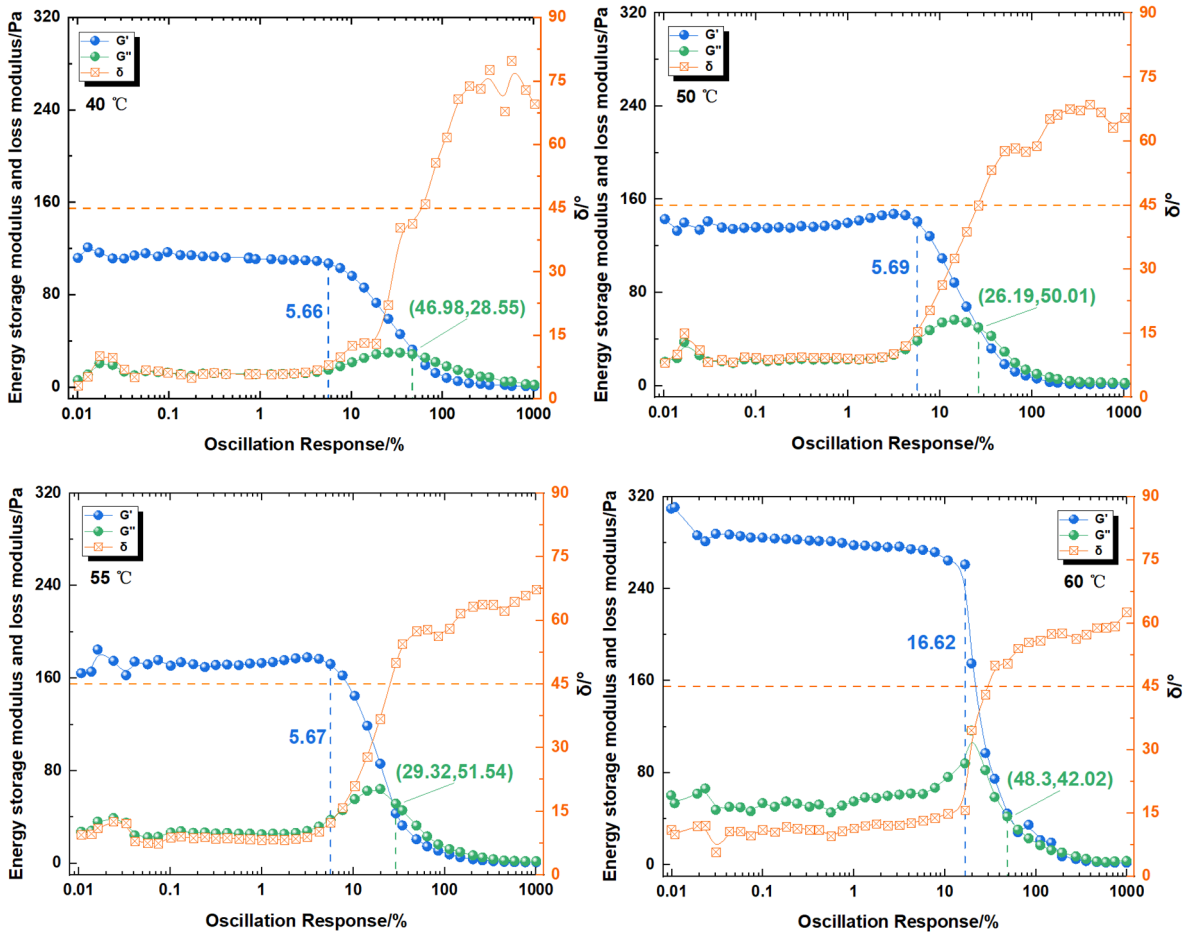

Figure 5. Changes in G′, G″ and δ with oscillatory strain in thermosensitive gel foam at different temperatures.

Overall, the G′ and G″ values of the foam at 60 °C in the linear viscoelastic range are significantly higher than those at other temperatures. This is because the gel foam at 60 °C has formed a cross-linked network structure inside, with more energy absorption points. The foam can effectively disperse and absorb energy when subjected to external forces, improving the overall energy storage and loss capabilities of the foam. The specific mechanism can be described as follows (see Figure 6): At a low temperature, the methoxy group (–OCH_3) on the MC molecular chain forms a hydrogen bond with water, and the molecule is fully solvated and in a dissolved state. When the temperature is raised to the critical gelation temperature (60 °C), the hydrophobicity of –OCH_3 is enhanced, the hydrogen bond formed with water is broken, and the in-termolecular hydrophobic association dominates, forming a three-dimensional network structure. At the same time,

the $B_4O_7^{2-}$ formed by the dissociation of sodium tetraborate in water undergoes hydrolysis to generate $B(OH)_{4^-}$, which can quickly react with the exposed -OH on the MC molecular chain to generate a large number of -B–O–C-cross-linked structures, thus building a highly dense viscoelastic network and causing the solution to gel.

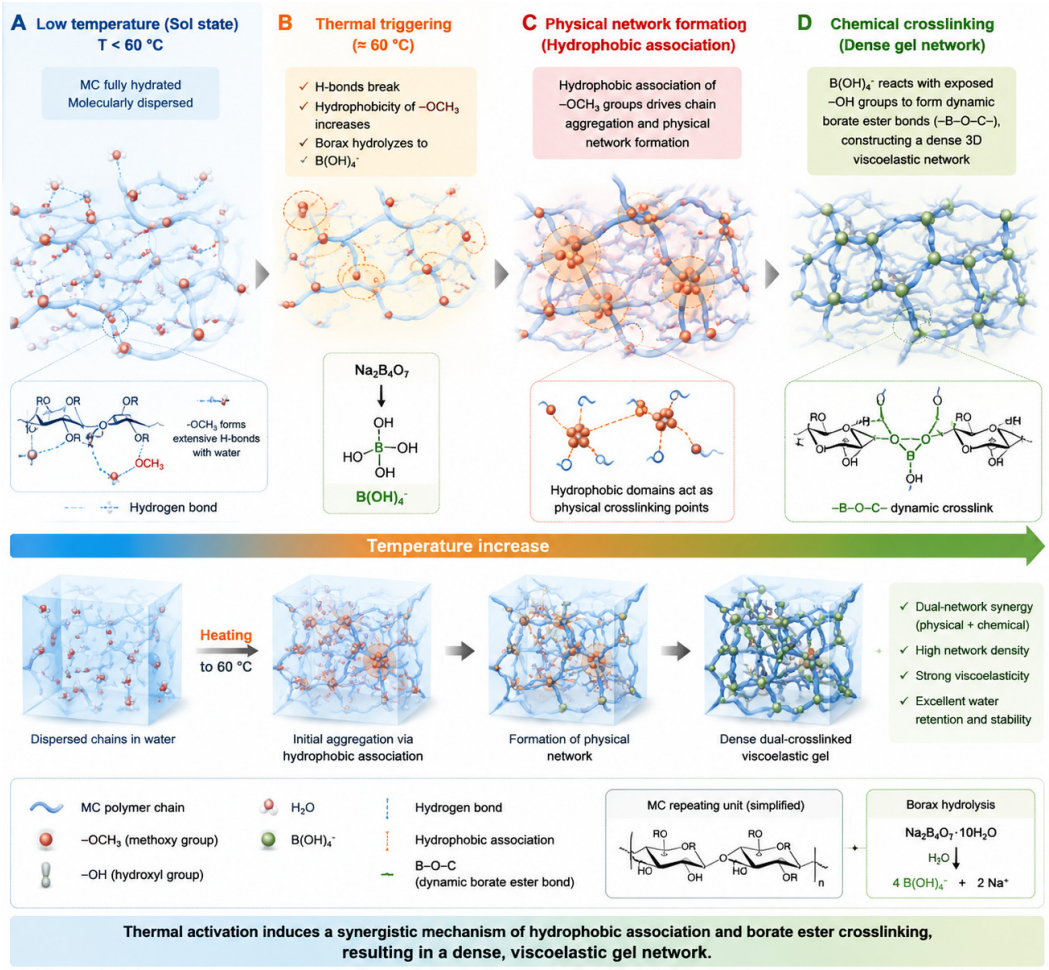

Figure 6. Phase-change mechanism of MC-based thermosensitive gel foam.

3.4. Effect of Foaming Ratio on Rheology of Thermosensitive Gel Foam

As shown in Figures 7 and 8, the shear rate–shear stress and shear rate–shear viscosity curves of gel foam show nonlinear increasing and decreasing trends, respectively, indicating that it is a typical non-Newtonian shear-thinning fluid. Especially in the low-shear-rate area (0–10 s^{-1}), the increase in shear stress and the decrease in apparent viscosity are large. In the high-shear-rate area (>50 s^{-1}), however, the increase in shear stress and the decrease in apparent viscosity tend to be gentle, indicating that the molecular chain orientation in the gel foam and the three-dimensional structure of the gel begin to adjust at low shear rates. At higher shear rates, the molecular chain orientation in the foam and the three-dimensional structure of the gel are destroyed, resulting in a reduction in its flow resistance until it reaches a relatively stable state. This shows that the restrictive effect of the internal structure of the foam on the flow is weakened, showing obvious shear thinning characteristics. The shear stress at 60 °C is significantly higher than that at 40 °C, indicating that the increase in temperature enhances the viscoelasticity of the gel foam system. At 60 °C, foams with larger expansion ratios have the highest shear stress, exhibiting higher structural rigidity. At 40 °C, however, the overall shear stress is smaller, especially in the low-shear-rate zone, indicating poor foam stability.

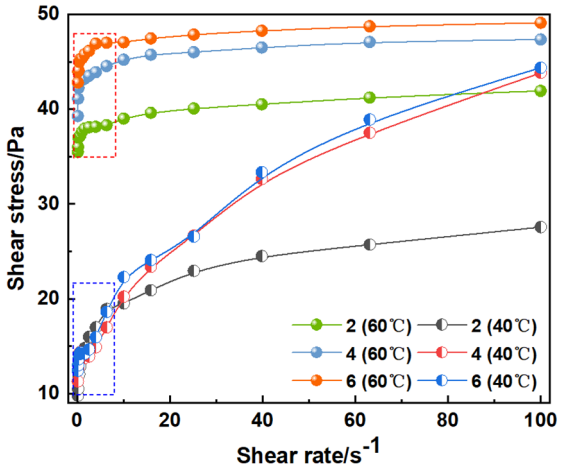

Figure 7. Effect of foaming ratio on foam shear stress under different temperature conditions.

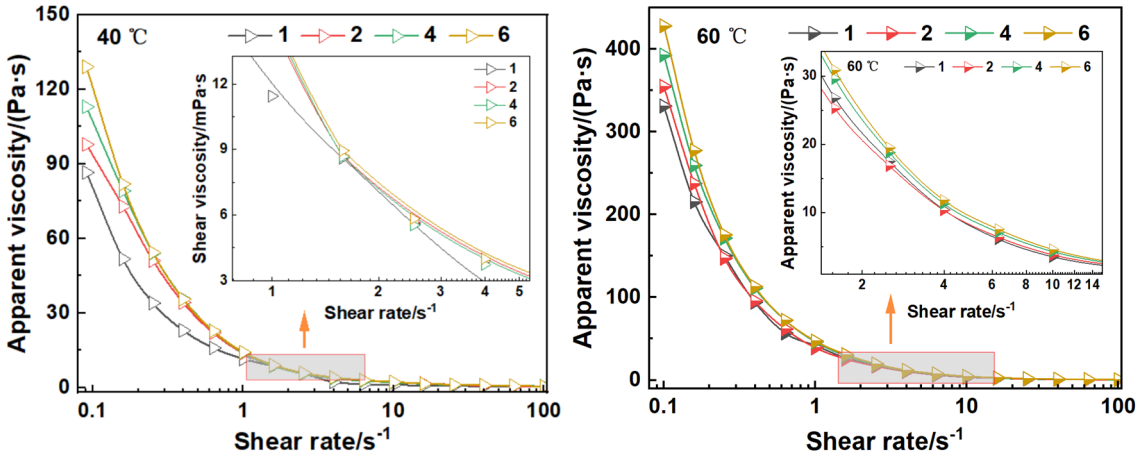

Figure 8. Effect of foaming ratio on foam shear viscosity under different temperature conditions.

As can be seen from the data within the red and blue dashed boxes in the low-shear-rate range (0–10 s^{-1}) in Figure 7, at 40 °C, the shear stress of the foam increases significantly as the shear rate increases; however, the expansion ratio has little effect on this increase in shear stress. It is worth noting that at low shear rates (0–10 s^{-1}), the foam shear stress at 40 °C is significantly lower than that at 60 °C. This indicates that the gel foam structure is more sensitive to low-speed flow under low-temperature conditions. Under high-temperature conditions, the internal molecules of the foam begin to cross-link and gel, making the system highly rigid. Under high-shear-rate (10–100 s^{-1}) conditions, an increase in temperature or expansion ratio can significantly increase the shear stress of the foam. It is worth noting that when the foam expansion ratio increases from two to four, the shear stress increases significantly, whereas when the foam expansion ratio increases from four to six, the increase in shear stress is significantly smaller. In particular, the shear stresses corresponding to the foam expansion ratios of four and six differ only slightly at 40 °C.

Similarly, at a specific shear rate, the apparent viscosity of the foam fluid also increases with the increase in the foaming multiple, and when the foaming multiple is higher, the viscosity increase also decreases significantly (See Figure 8). This is because the number of bubbles in foam with a high foaming ratio increases, the bubble size is smaller, and the contact area between the bubbles is larger. The obstruction effect is more significant during the foam flow process, resulting in an increase in shear stress and apparent viscosity. However, when the foaming ratio increases to a certain value, the increase in shear stress

and apparent viscosity will decrease. This is mainly because the liquid film of foam with a high foaming ratio is thinner and more susceptible to disturbance and rupture, which will reduce the flow resistance between the bubbles, thereby offsetting the increase in shear stress and apparent viscosity caused by the increase in the number of foams and their reduction in size [6].

3.5. Effect of Inorganic Salt Ions on the Rheology of Gel Foam

As shown in Figure 9, in the foam system containing $CaCl_2$ and NaCl, the apparent viscosity of the gel foam shows typical shear-thinning characteristics as the shear rate increases, and the difference is most significant in the low-shear-rate region (0.1–1 s^{-1}). Overall, at 40 °C and a low shear rate, the apparent viscosity of the foam system containing 100 mg/L $CaCl_2$ is 143.807 mPa·s, and when it contains 1000 mg/L $CaCl_2$, it drops to 59.3338 mPa·s, a decrease of 58.74%. At 60 °C, the difference tends to shrink, containing 100 mg/L. The apparent viscosity of the CaCl2 foam system is 367.219 mPa·s, while it drops to approximately 192.052 mPa·s at a concentration of 1000 mg/L, a decrease of 47.7%. It is worth noting that at 40 °C and 60 °C, when the $CaCl_2$ concentration increases from 100 mg/L to 200 mg/L, the apparent viscosity of the gel foam increases slightly. This is because the increase in $CaCl_2$ concentration significantly weakens the apparent viscosity level of the system, and this effect is more obvious under low-temperature conditions. This is because the divalently charged Ca^{2+} can form an ionic bridge structure with oxygen-containing functional groups (such as hydroxyl groups, ether oxygen groups, etc.) in the system, which helps to build a denser three-dimensional network at low concentrations, thereby improving the strength and structural stability of the foam liquid film. However, as the concentration increases, excess Ca^{2+} triggers a strong charge-shielding effect, destroys the original hydrogen bonds and association structures, and changes the network from "bridging enhancement" to "structural deconstruction". This results in a loose foam skeleton and accelerated liquid-film drainage, thereby significantly reducing the apparent viscosity. In addition, at 60 °C, although the thermal movement of molecules in the foam system is enhanced and the chain segments are significantly relaxed, the high temperature induces phase change and gelation of the thermosensitive foam, which increases the cross-linking effect between molecules in the system and weakens the damage of Ca^{2+} to the foam structure to a certain extent.

As shown in Figure 9 c and d, the NaCl system also exhibits shear-thinning behavior in which the apparent viscosity decreases as the shear rate increases, but the overall apparent viscosity is significantly lower than that of the gel foam system containing $CaCl_2$. Similar to the foam system containing $CaCl_2$, under the low-shear-rate condition of 40 °C, the apparent viscosity of the foam system containing 100 mg/L of NaCl is 127.807 mPa·s. Meanwhile, it drops to 57.097 mPa·s when containing 1000 mg/L NaCl, a decrease of 55.33%. At 60 °C, the difference tends to shrink, containing 100 mg/L. The apparent viscosity of the NaCl foam system is 263.816 mPa·s, but at a concentration of 1000 mg/L it drops to about 143.960 mPa·s, a decrease of more than 45.43%. Unlike the foam system containing $CaCl_2$, the apparent viscosity of the gel foam containing NaCl gradually decreases with the increase in inorganic salt concentration under low-shear-viscosity conditions of 40 °C and 60 °C, and there is no phenomenon of first increasing and then decreasing. This shows that the increase in NaCl concentration also significantly weakens the apparent viscosity of the foam system, but its ability to strengthen the overall structure of the foam system is weaker than that of $CaCl_2$. This behavior can be attributed to the coupled effects of NaCl on MC hydration and gas–liquid interfacial interactions. As a salting-out electrolyte, NaCl alters the hydration and intermolecular association of MC, thereby regulating its network organization and rheological behavior [37,38]. Meanwhile, increased ionic strength compresses

the electrical double layer at charged gas–liquid interfaces, reducing electrostatic repulsion and promoting liquid-film thinning and drainage, which can weaken foam stability [39]. Therefore, the viscosity reduction at elevated NaCl concentrations is more reasonably ascribed to salt-induced changes in MC hydration/association and foam–film stability rather than direct electrostatic screening between MC chains.

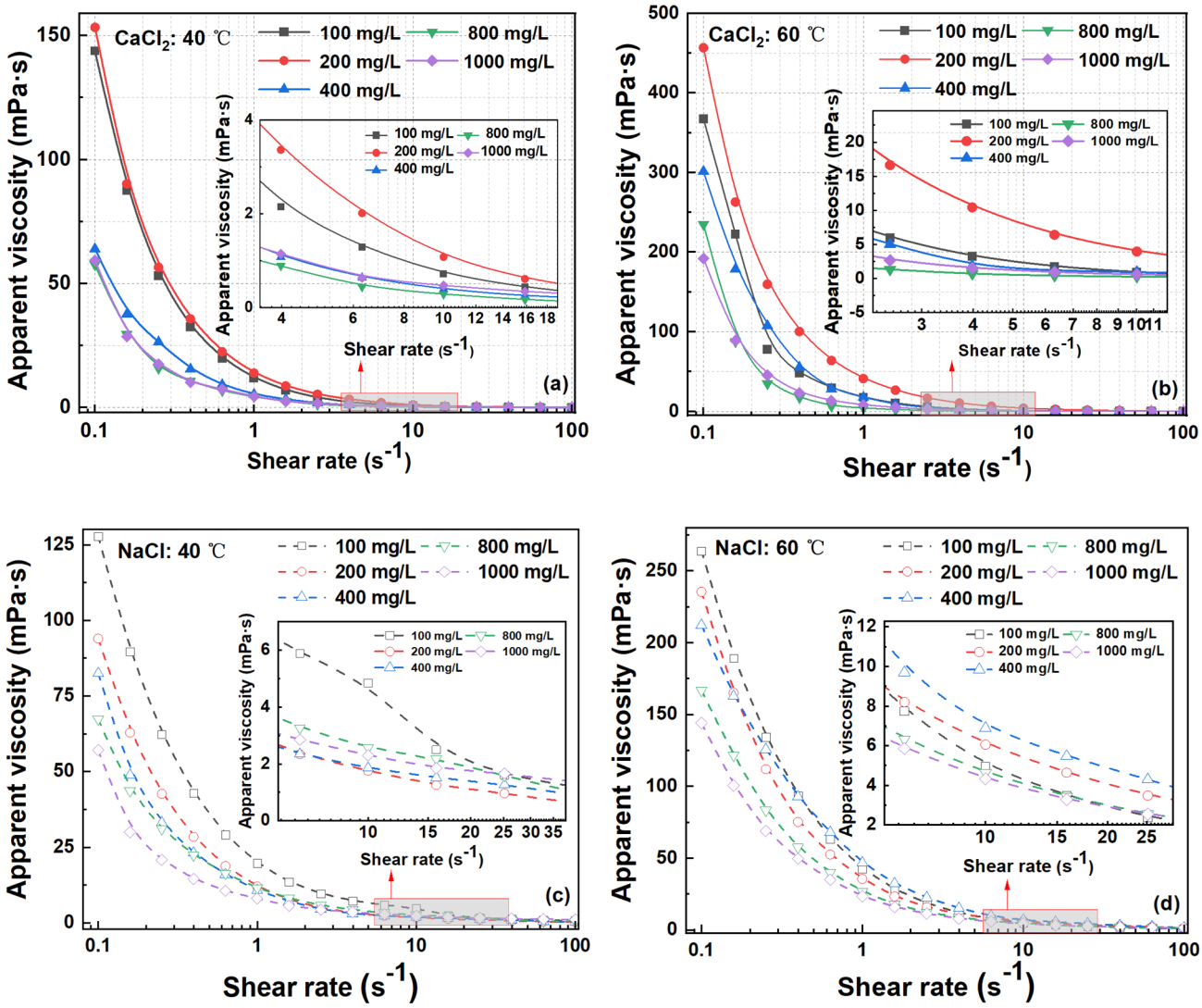

Figure 9. Effect of inorganic salts on foam shear viscosity. (**a**) $CaCl_2$/40 °C, (**b**) $CaCl_2$/60 °C, (**c**) NaCl/40 °C, (**d**) NaCl/60 °C.

As shown in Figure 10, the distinct effects of Na^+ and Ca^{2+} are further associated with their different valence and hydration characteristics, which regulate the local aqueous environment, polymer association, and water distribution. Upon heating, progressive dehydration of MC enhances the hydrophobic association between methoxy-rich segments, forming physical junctions and eventually a three-dimensional network [26]. At approximately 60 °C, this thermally induced network formation markedly enhances the viscosity and viscoelasticity of the gel foam. Borate-mediated interactions with accessible hydroxyl groups may further reinforce the network. Thus, the enhanced viscoelasticity at 60 °C is attributed to the synergistic effects of thermally induced MC hydrophobic association and borate-assisted network formation.

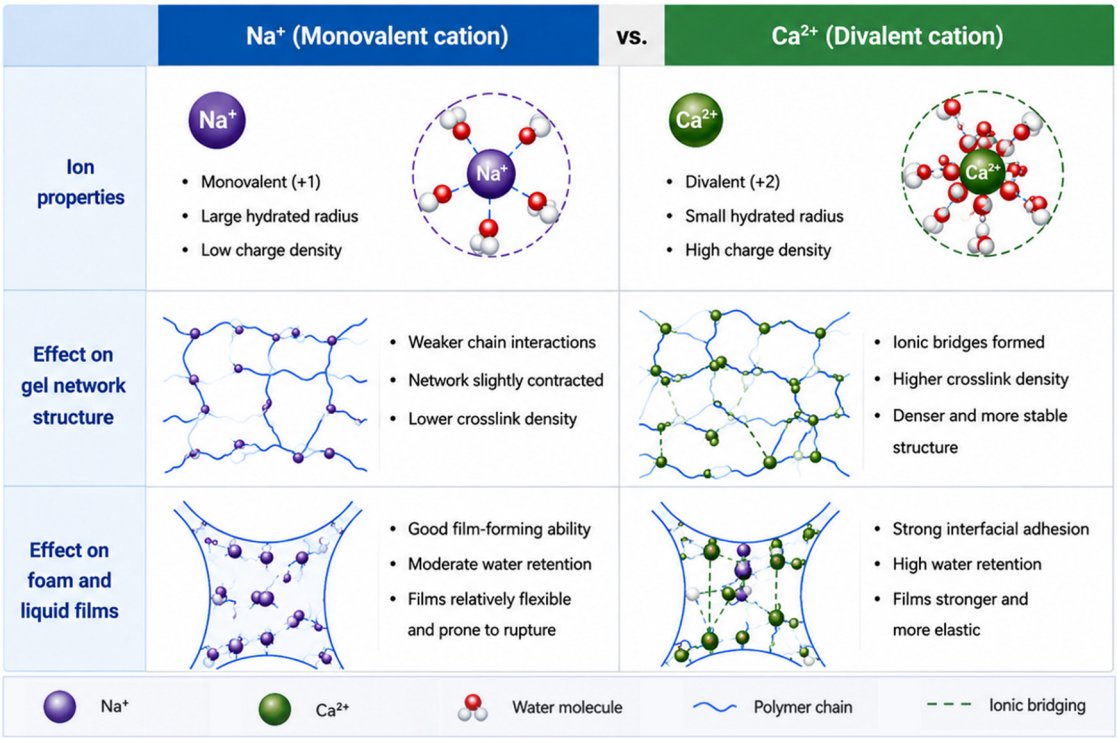

Figure 10. Mechanism of the influence of different salt ions on the rheological properties of gel foam.

3.6. Gel Foam Fluidity and Water Retention and Film-Forming Properties

3.6.1. Osmotic Flow Properties of Gel Foam

As shown in Figure 11, the mass of gel foam exuded under different ionic systems showed an "S"-shaped increase over time, with, roughly, an initial slow exudation stage (0 to 20 min), a rapid exudation stage (20 to 60 min), and a stable stage (60 to 100 min). In the initial stage, the exudation quality of the three systems was low, less than 30 g at 20 min, indicating that in the early stage the foam was mainly retained inside the coal particles, and the foam migrated slowly; as time went on, the foam gradually overcame the constraints of viscosity and capillary force under the action of gravity, and began to exude in large quantities. At 100 min, the exudation masses of the gel foam containing NaCl and $CaCl_2$ were 211.42 g and 209.48 g respectively, approximately 11.54% and 10.52% higher than the ion-free system, respectively. At the same time, between 25 and 35 min, the exudation rate of the foam in the salt-containing system was significantly higher than that in the ion-free system, with the NaCl system always showing the largest amount of exudation, indicating that the presence of inorganic salt ions weakens the retention of gel foam within coal particles and promotes the migration rate of the foam.

As shown in Figure 11, the cumulative exudation followed the order NaCl > $CaCl_2$ > salt-free system, indicating that inorganic salts promoted short-term liquid migration from the gel foam within coal particles. This behavior can be attributed to the coupled effects of salt-induced changes in MC hydration/network organization and foam–film interactions. Previous studies have demonstrated that the gelation and mechanical properties of MC are strongly dependent on ion type and concentration, owing to ion-specific regulation of polymer hydration and association [40,41]. Meanwhile, electrolytes can modify interfacial interactions, film thinning, and drainage, thereby altering foam stability [42]. The difference between NaCl and $CaCl_2$ is likely associated with their distinct ionic characteristics and resulting effects on the aqueous and polymer environments. NaCl primarily alters MC hydration and network organization without providing sufficient structural stabilization to restrict liquid migration, resulting in the highest exudation. In contrast, $CaCl_2$ exerts a

stronger influence on the hydration environment and polymer organization because of the divalent nature of Ca^{2+}, thereby partially restricting liquid mobility and reducing exudation relative to NaCl [40]. Studies of cellulose-ether systems have confirmed that NaCl and $CaCl_2$ distinctly regulate their phase transition and viscoelastic properties, while structural investigations of MC gels further demonstrate substantial salt-induced reorganization of the fibrillar network [41]. Consequently, the intermediate exudation of the $CaCl_2$ system likely reflects a balance between salt-induced enhancement of short-term liquid mobility and ion-specific regulation of hydration and network organization. Thus, the increased exudation of the salt-containing foams reflects enhanced short-term liquid migration and should not be interpreted as necessarily indicating poorer long-term water retention.

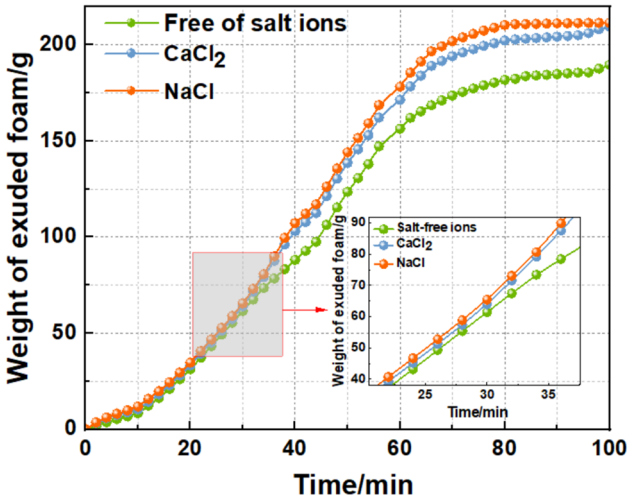

Figure 11. Changes in gel foam exudation quality over time.

3.6.2. Gel Foam Water Retention and Film-Forming Properties

As shown in Figure 12, all gel foams exhibited a two-stage mass-loss behavior, with rapid water loss during the first day followed by a slower decay. After 1 day, the remaining masses of the salt-free, NaCl, and $CaCl_2$ systems were 81.05, 82.25, and 86.71 g, respectively, corresponding to mass losses of 18.95%, 17.75%, and 13.29%. By day 6, the remaining masses decreased to 70.30, 73.69, and 78.27 g, respectively, demonstrating that both salts suppressed long-term water loss, with $CaCl_2$ exhibiting the strongest retention effect. The different effects of NaCl and $CaCl_2$ can be attributed to their ion-specific regulation of MC hydration, network organization, and water mobility [37,40]. NaCl modifies the hydration environment and intermolecular association of MC, thereby providing moderate resistance to water migration.

In contrast, the divalent Ca^{2+}, owing to its higher charge density and stronger hydration characteristics, exerts a more pronounced influence on the local water environment and salt-induced reorganization of the MC network [40,41]. These effects collectively enhance water immobilization and retard long-term water loss, accounting for the superior retention of the $CaCl_2$-containing foam. This result does not contradict the higher short-term exudation observed in Figure 11: exudation primarily reflects rapid liquid redistribution and drainage within coal particles, whereas the mass-retention test characterizes long-term water loss governed by evaporation, water immobilization, and gradual network relaxation. Thus, inorganic salts can facilitate initial liquid redistribution while simultaneously improving long-term water retention, with $CaCl_2$ providing the stronger overall retention effect.

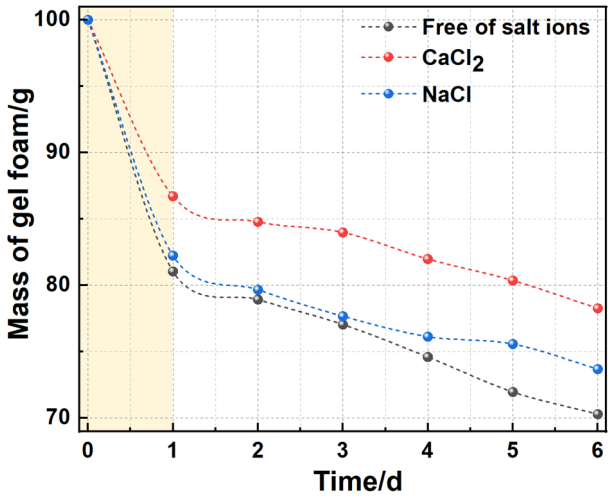

Figure 12. Gel foam water retention.

As shown in Figure 13, the salt-free foam maintained a fine and homogeneous structure after 72 h, with a continuous and compact surface film and no visible collapse or cracking, indicating superior film-forming ability. In contrast, the $CaCl_2$-containing foam exhibited pronounced surface embrittlement and through-cracks. This behavior is likely associated with the strong ion-specific effect of Ca^{2+} on MC hydration and network organization. Owing to its higher charge density and stronger ion–water interactions, Ca^{2+} induces more pronounced redistribution of water and structural reorganization within the polymer network. During prolonged water loss, spatially heterogeneous network contraction may generate localized internal stresses, eventually leading to film embrittlement and cracking.

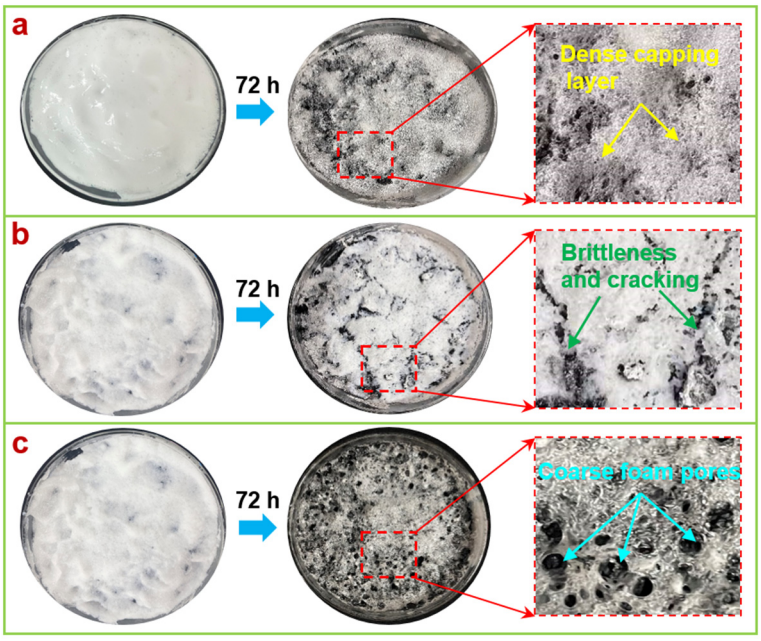

Figure 13. Film-forming performance of different thermosensitive gels: (**a**) salt-free ionic system, (**b**) $CaCl_2$, (**c**) NaCl.

The NaCl-containing foam showed no obvious brittle cracking but developed larger, interconnected pores and a less compact surface film. Compared with Ca^{2+}, Na^{+} exerts a weaker influence on the hydration environment and network organization, providing insufficient structural reinforcement to suppress liquid drainage and bubble coalescence.

Consequently, progressive film thinning and bubble coarsening facilitate the formation of large, interconnected pores and compromise surface-film integrity.

Overall, the salt-free foam exhibited the highest film-forming integrity but relatively poor water retention, whereas the addition of NaCl or $CaCl_2$ improved water retention at the expense of surface-film compactness. Notably, the distinct morphologies of the NaCl and $CaCl_2$ systems indicate different salt-dependent structural evolution pathways: NaCl primarily promotes film thinning and pore coarsening, whereas $CaCl_2$ induces stronger network reorganization and heterogeneous shrinkage during prolonged water loss. These findings demonstrate that gel-foam stability is governed by the coupled evolution of polymer-network organization, interfacial film integrity, water mobility, and bubble structure, rather than by film-forming ability or water retention alone.

4. Conclusions

This study systematically investigated the effects of temperature, foaming ratio, and inorganic salts on the rheological and functional properties of thermosensitive gel foam for coal-fire prevention. The main conclusions are as follows:

(1) The thermosensitive gel foam exhibited typical yield–pseudoplastic behavior. Gelation at 60 °C markedly enhanced the apparent viscosity, whereas increasing shear induced pronounced shear thinning. The foaming ratio showed a threshold effect, with rheological enhancement approaching saturation at a foaming ratio of four.

(2) Among the Bingham, Power-law, and Herschel–Bulkley models, the Herschel–Bulkley model provided the most appropriate description of the flow behavior, with R^2 values above 0.9930. Its inclusion of yield stress and shear-thinning parameters also provides a physically meaningful representation of the structured gel foam.

(3) Gelation at 60 °C significantly enhanced the viscoelastic response of the foam. Compared with 40–55 °C, the linear viscoelastic region increased by approximately 11 percentage points, accompanied by higher G' and G'', indicating improved resistance to deformation and enhanced energy storage and dissipation.

(4) Inorganic salts produced distinct effects on water retention and film formation. The salt-free foam exhibited superior film-forming integrity, whereas NaCl and $CaCl_2$ improved long-term water retention, with $CaCl_2$ showing the stronger effect. These differences are associated with ion-specific regulation of MC hydration, network organization, water mobility, and interfacial film stability.

Author Contributions: Writing—original draft, J.G.; Writing—review and editing, J.G., B.Y. and N.Z.; Software, J.G., B.Y., N.Z., S.H., D.M. and X.Z.; Investigation, J.G., B.Y., N.Z., S.H., Y.C., F.T. and X.Z.; Methodology, J.G., D.M. and Y.C.; Conceptualization, J.G. and H.W.; Supervision, J.G. and H.W.; Data curation, J.G. and Y.C.; Validation, X.Z. All authors have read and agreed to the published version of the manuscript.

Funding: This research was funded by the National Natural Science Foundation of China (Grant No. 52574224), the Anhui Provincial Natural Science Foundation (Grant No. 2408085ME148), and the China Postdoctoral Science Foundation (Grant No. 2025MD774101).

Data Availability Statement: The data that support the findings of this study are available from the corresponding author upon reasonable request.

Conflicts of Interest: Author Ning Zhang was employed by the company Huayuan Mine, Jining Coal Mining Group Co., Ltd.; The remaining authors declare that the research was conducted in the absence of any commercial or financial relationships that could be construed as a potential conflict of interest.

References

1. Pei, X.; Chen, J.; Liu, H.; Wang, L.; Miao, Z.; Yuan, Y.; Xi, J.; Li, C.; Tian, C.; Liu, Y. Thermo-responsive hydroxypropyl methylcellulose and sodium alginate composite hydrogels and their fire extinguishing properties. *Fire* **2026**, *9*, 88. [CrossRef]
2. Shao, H.; Wang, Z.; Jiang, S.; Zhang, Y.; Xi, X.; Wu, Z. Mining polyethylene glycol-based thermosensitive hydrogel materials: Preparation and flame re-tardant properties. *ACS Omega* **2023**, *8*, 5947–5957. [CrossRef]
3. Shi, G.-Q.; Wang, G.-Q.; Ding, P.-X.; Wang, Y.-M. Model and simulation analysis of fire development and gas flowing influenced by fire zone sealing in coal mine. *Process Saf. Environ. Prot.* **2021**, *149*, 631–642. [CrossRef]
4. Ma, X.; Fang, Y.; Wu, R.; Yang, L.; Wang, Y.; Yuan, B. Fire warning sensing materials: Advances, prospects, and challenges. *Emerg. Manag. Sci. Technol.* **2025**, *5*, e005. [CrossRef]
5. Shi, Q.; Long, L.; Sun, Y.; Zhao, S.; Pang, Y.; Xia, C. Formation mechanism and the extinguishment performance of gel-stabilized foam for inhibiting coal spontaneous combustion. *Energy* **2024**, *303*, 131995. [CrossRef]
6. Xue, D.; Hu, X.; Cheng, W.; Wei, J.; Zhao, Y.; Shen, L. Fire prevention and control using gel-stabilization foam to inhibit spontaneous combustion of coal: Characteristics and engineering applications. *Fuel* **2020**, *264*, 116903. [CrossRef]
7. Zhang, Y.; You, F.; Huang, H.; Wang, Z.; Liu, D. Bio-based L-lysine phosphate/dicyandiamide/silica sol composite system for highly efficient green flame retardancy of cotton fabrics. *Emerg. Manag. Sci. Technol.* **2025**, *5*, e026. [CrossRef]
8. Tang, Z.; Xu, G.; Yang, S.; Deng, J.; Xu, Q.; Chang, P. Fire-retardant foam designed to control the spontaneous combustion and the fire of coal: Flame re-tardant and extinguishing properties. *Powder Technol.* **2021**, *384*, 258–266. [CrossRef]
9. Lu, Y.; Liu, Y.; Shi, S.; Wang, G.G.; Li, H.; Wang, T. Micro-particles stabilized aqueous foam for coal spontaneous combustion control and its flow character-istics. *Process Saf. Environ. Prot.* **2020**, *139*, 262–272. [CrossRef]
10. Ray, S.K.; Singh, R.P. Recent developments and practices to control fire in undergound coal mines. *Fire Technol.* **2007**, *43*, 285–300. [CrossRef]
11. Smith, A.C.; Trevits, M.A.; Mucho, T.P. Evaluation of gas-enhanced foam for suppressing coal mine fires. In *Proceedings of the National Coal Show, Pittsburgh, Pennsylvania, 7–9 June 2005*; Mining Media, Inc.: Denver, CO, USA, 2005.
12. Fan, X.; Ma, L.; Sheng, Y.; Liu, X.; Wei, G.; Liu, S.; Zhang, J. Gel foam technologies for preventing coal spontaneous combustion: A review. *Combust. Sci. Technol.* **2026**, *198*, 569–599. [CrossRef]
13. Qin, B.; Lu, Y.; Li, Y.; Wang, D. Aqueous three-phase foam supported by fly ash for coal spontaneous combustion prevention and control. *Adv. Powder Technol.* **2014**, *25*, 1527–1533. [CrossRef]
14. Qin, B.; Jia, Y.; Lu, Y.; Li, Y.; Wang, D.; Chen, C. Micro fly-ash particles stabilized Pickering foams and its combustion-retardant characteristics. *Fuel* **2015**, *154*, 174–180. [CrossRef]
15. Lu, Y. Laboratory study on the rising temperature of spontaneous combustion in coal stockpiles and a paste foam suppression tech-nique. *Energy Fuels* **2017**, *31*, 7290–7298. [CrossRef]
16. Shi, Q.; Qin, B.; Hao, Y.; Li, H. Experimental investigation of the flow and extinguishment characteristics of gel-stabilized foam used to control coal fire. *Energy* **2022**, *247*, 123484. [CrossRef]
17. Xu, Y.; Qin, B.; Shi, Q.; Liu, H. Rheological Characterization of Inorganic Curing Foam for Preventing Spontaneous Combustion of Coal. *Combust. Sci. Technol.* **2025**, *197*, 5079–5097. [CrossRef]
18. Hao, M.; Qin, B.; Shi, Q.; Wang, S. The preparation and characteristics of mining waste-derived thermoresponsive hydrogel used for coal fire suppression. *Colloids Surf. A Physicochem. Eng. Asp.* **2025**, *725*, 137644. [CrossRef]
19. Huang, X.; Ma, L.; He, C.; Wei, G.; Pang, J.; Guo, R.; Zhao, Y. Synthesis and characteristics of thermosensitive hydrogel for extinguishing coal mines fire. *Combust. Sci. Technol.* **2025**, *197*, 6339–6358. [CrossRef]
20. Zhou, G.; Li, S.; Meng, Q.; Tian, F.; Sun, L. Synthesis and performance of a new temperature-sensitive and super-absorbent fire prevention hy-drogel based on ultrasonic method. *Colloids Surf. A Physicochem. Eng. Asp.* **2022**, *640*, 128399. [CrossRef]
21. Ma, H.; Gan, J.; Zhang, J. Study on preparation of temperature-sensitive foam gel for mine fire prevention and extinguishing. *Coal Technol.* **2026**, *45*, 151–155.
22. Li, Y. Quantitative inversion model design of mine water characteristic ions based on hyperspectral technology. *Sci. Program.* **2022**, *2022*, 5747974. [CrossRef]
23. Gan, J.; Zhong, S.; Zhang, J.; Zhang, L.; Wang, H.; Wang, D. Mechanistic insights into coal wettability modulation by surfactants with varied hydrophilic group counts. *Fuel* **2026**, *405*, 136658. [CrossRef]
24. Gan, J.; Wang, D.; Xiao, Z.; Wang, Y.-N.; Zhang, K.; Zhu, X.; Li, S. Experimental and molecular dynamics investigations of the effects of ionic surfactants on the wetta-bility of low-rank coal. *Energy* **2023**, *271*, 127012. [CrossRef]
25. Haque, A.; Morris, E.R. Thermogelation of methylcellulose. Part I: Molecular structures and processes. *Carbohydr. Polym.* **1993**, *22*, 161–173. [CrossRef]
26. Desbrieres, J.; Hirrien, M.; Ross-Murphy, S.B. Thermogelation of methylcellulose: Rheological considerations. *Polymer* **2000**, *41*, 2451–2461, Correction in *Polymer* **2000**, *41*, 5547. [CrossRef]
27. Li, L.; Shan, H.; Yue, C.Y.; Lam, Y.C.; Tam, K.C.; Hu, X. Thermally Induced Association and Dissociation of Methylcellulose in Aqueous Solutions. *Langmuir* **2002**, *18*, 7291–7298. [CrossRef]

28. Knarr, M.; Bayer, R. The shear dependence of the methylcellulose gelation phenomena in aqueous solution and in ceramic paste. *Carbohydr. Polym.* **2014**, *111*, 80–88. [CrossRef] [PubMed]
29. Zhang, P.; Ma, Z.; Bai, Z.; Ye, J. Rheological and energy transport characteristics of a phase change material slurry. *Energy* **2016**, *106*, 63–72. [CrossRef]
30. Phuoc, T.X.; Wang, P.; McIntyre, D.; Shadle, L. Synthesis and characterization of a thixotropic coal–water slurry for use as a liquid fuel. *Fuel Process. Technol.* **2014**, *127*, 105–110. [CrossRef]
31. Ma, F.; Zhang, P. A review of thermo-fluidic performance and application of shellless phase change slurry: Part 2–Flow and heat transfer characteristics. *Energy* **2020**, *192*, 116602. [CrossRef]
32. Balmforth, N.J.; Frigaard, I.A.; Ovarlez, G. Yielding to stress: Recent developments in viscoplastic fluid mechanics. *Annu. Rev. Fluid Mech.* **2014**, *46*, 121–146. [CrossRef]
33. Stewart, P.S.; Hilgenfeldt, S. Gas-Liquid Foam Dynamics: From Structural Elements to Continuum Descriptions. *Annu. Rev. Fluid Mech.* **2023**, *55*, 323–350. [CrossRef]
34. Faroughi, S.A.; Pruvot, J.C.J.; Mcandrew, J. The rheological behavior of energized fluids and foams with application to hydraulic fracturing: Review. *J. Pet. Sci. Eng.* **2017**, *163*, 243–263. [CrossRef]
35. Wang, H.; Wei, X.; Du, Y.; Wang, D. Experimental investigation on the dilatational interfacial rheology of dust-suppressing foam and its effect on foam performance. *Process Saf. Environ. Prot.* **2019**, *123*, 351–357. [CrossRef]
36. Celik, F.; Canakci, H. An investigation of rheological properties of cement-based grout mixed with rice husk ash (RHA). *Constr. Build. Mater.* **2015**, *91*, 187–194. [CrossRef]
37. Xu, Y.; Li, L.; Zheng, P.; Lam, Y.C.; Hu, X. Controllable gelation of methylcellulose by a salt mixture. *Langmuir* **2004**, *20*, 6134–6138. [CrossRef] [PubMed]
38. Kundu, P.P.; Kundu, M. Effect of salts and surfactant and their doses on the gelation of extremely dilute solutions of methyl cellulose. *Polymer* **2001**, *42*, 2015–2020. [CrossRef]
39. Wang, L.; Yoon, R.H. Effect of pH and NaCl concentration on the stability of surfactant-free foam films. *Langmuir* **2009**, *25*, 294–297. [CrossRef] [PubMed]
40. Almeida, N.; Rakesh, L.; Zhao, J. Phase behavior of concentrated hydroxypropyl methylcellulose solution in the presence of mono and divalent salt. *Carbohydr. Polym.* **2014**, *99*, 630–637. [CrossRef] [PubMed]
41. Liberman, L.; Schmidt, P.W.; Coughlin, M.L.; Ya'aKobi, A.M.; Davidovich, I.; Edmund, J.; Ertem, S.P.; Morozova, S.; Talmon, Y.; Bates, F.S.; et al. Salt-dependent structure in methylcellulose fibrillar gels. *Macromolecules* **2021**, *54*, 2090–2100. [CrossRef]
42. Angarska, J.; Tachev, K.; Kralchevsky, P.; Mehreteab, A.; Broze, G. Effects of Counterions and Co-ions on the Drainage and Stability of Liquid Films and Foams. *J. Colloid Interface Sci.* **1998**, *200*, 31–45. [CrossRef]

Disclaimer/Publisher's Note: The statements, opinions and data contained in all publications are solely those of the individual author(s) and contributor(s) and not of MDPI and/or the editor(s). MDPI and/or the editor(s) disclaim responsibility for any injury to people or property resulting from any ideas, methods, instructions or products referred to in the content.